

Tunnelling in quantum superlattices with variable lacunarity

Francisco R. Villatoro¹ and Juan A. Monsoriu^{2*}

¹ Departamento de Lenguajes y Ciencias de la Computación, Universidad de Málaga, E-29071 Málaga, Spain

² Departamento de Física Aplicada, Universidad Politécnica de Valencia, E-46022 Valencia, Spain

Abstract. Quantum fractal superlattices are microelectronic devices consisting of a series of thin layers of two semiconductor materials deposited alternately on each other over a substrate following the rules of construction of a fractal set, here, a symmetrical polyadic Cantor fractal. The scattering properties of electrons in these superlattices may be modeled by using that of quantum particles in piecewise constant potential wells. The twist plots representing the reflection coefficient as function of the lacunarity parameter show the appearance of black curves with perfectly transparent tunnelling which may be classified as vertical, arc, and striation nulls. Approximate analytical formulae for these reflection-less curves are derived using the transfer matrix method. Comparison with the numerical results show their good accuracy.

PACS numbers: 03.65.Nk, 05.45.Df

Submitted to: *Eur. J. Phys.*

* To whom correspondence should be addressed (jmonsoni@fis.upv.es)

1. Introduction

Quantum superlattices are microelectronic devices composed of alternating layers of two semiconductors with different energy band gaps deposited over a substrate [1, 2, 3, 4]. The sandwiching of two materials whose band gap energies are different results in a rectangular potential well for the electrons (holes) in the conduction (valence) band. The thickness of each semiconductor layer is about 10–100 atoms (1–10 nm), so this three-dimensional finite potential well may be split into a two-dimensional system in the transversal dimensions, where electrons behave as a two-dimensional electron gas with continuous energy states, and a one-dimensional finite square well in the growth direction with discrete bound states.

In the absence of external electric field, semiconductor superlattices may be considered, in the first approximation, as quasi-one-dimensional system of rectangular quantum wells separated by potential barriers (in the conduction band). When an external force is applied to the electrons in the quantum-well heterostructure they do not respond as free particles due to the influence of the other atoms. These effects may be taken into account by introducing an “effective mass” (m^*) which relates the particle motion to an external force (or potential) without worrying about all the atomic forces. Therefore, the scattering in semiconductor superlattices can be easily solved by means of the transfer matrix method using an effective mass for the electrons [5, 6, 7, 8, 9].

Fractal superlattices are designed by alternating semiconductor materials according to an iterative fractal process using techniques such as molecular beam epitaxy [10]. These devices may be crystalline or amorphous. A typical device for the first kind is made by several layers of gallium arsenide (GaAs) of a few Angstrom (Å) thick sandwiched between aluminium gallium arsenide ($\text{Al}_x\text{Ga}_{1-x}\text{As}$) ones, where the crystal composition x may vary between 0 and 1, such as those fabricated by Axel and Terauchi [11] using $x = 0.3$, corresponding to a monolayer of $\text{Al}_x\text{Ga}_{1-x}\text{As}$ with thickness of 0.28 nm. A typical amorphous device is made by alternating layers of amorphous germanium (a-Ge) and amorphous silicon (a-Si) deposited in a silicon substrate [12], each layer having a thickness of less than 1.4 nm with good sharpness.

The scattering of electrons in symmetrical polyadic Cantor fractal potentials, characterized by a lacunarity parameter which is independent of their fractal dimension, have been numerically obtained by means of the transfer matrix method in Ref. [13]. The representation of the reflection coefficient as a function of the particle energy and the lacunarity shows perfectly transparent tunneling along some curves, referred to as nulls, which may be classified as vertical (lacunarity-independent), arc (concave upward), and striation (concave downward) nulls [14]. Analytical expressions for the position of these nulls have been obtained in Ref. [14] in an optical context, which may be properly adapted to the present application. However, those authors omit the details of their derivation which may be of great interest when quantum fractal superlattices are incorporated as laboratory assignments [13, 15].

In his paper, the transfer matrix method is used to obtain analytical expressions



Figure 1. First two stages ($S = 1$ and $S = 2$) of polyadic Cantor fractal sets with $N = 5$ (a) and $N = 6$ (b), showing the definition of both the scale factor (γ) and the lacunarity parameter (ε). Black and white regions denote the potential values $-V$ and 0 , respectively.

for the reflection-less energies of particles in fractal superlattices designed as polyadic Cantor sets with variable lacunarity. The contents of this paper are as follows. The next section recalls the main facts about these kind of fractal superlattices. Section 3, presents the analytical formulas for the reflection-less energies, whose validity is shown in Section 4 by its comparison with numerical results. Finally, the last section is devoted to the main conclusions.

2. Polyadic Cantor superlattices

In Cantor superlattices the distribution of the layers' thickness along growth axis corresponds to a finite order approximation to a polyadic, or generalized, Cantor set [16, 17]. These sets are defined as follows. The first step ($S = 0$) is to take a segment of unit length, referred to as initiator. In the next step, $S = 1$, the segment is replaced by N non-overlapping copies of the initiator, each one scaled by a factor $\gamma < 1$. For even N , as shown in Fig. 1(b), one half of the copies are placed completely to the left of the interval and the other half completely to its right, each copy being separated by a fixed distance, let us say ε . For odd N , as shown in Fig. 1(a), one copy lies exactly centered in the interval, and the rest ones are distributed as for even N , i.e., $\lfloor N/2 \rfloor$ copies are placed completely to the left of the interval and the other $\lfloor N/2 \rfloor$ copies wholly to its right, where $\lfloor N/2 \rfloor$ is the greatest integer less than or equal to $N/2$. At the following construction stages of the the fractal set, $S = 2, 3, \dots$, the generation process is repeated over and over again for each segment in the previous stage. Strictly speaking the Cantor set is the limit of this procedure for $S \rightarrow \infty$, which is composed of geometric points distributed such that each point lies arbitrarily close of other points of the set, being the S -th stage Cantor set usually referred to as a pre-fractal or physical fractal.

Symmetrical polyadic Cantor fractals are characterized by three parameters, the number of self-similar copies N , the scaling factor γ , and the width of the outermost gap at the first stage, ε , here on referred to as the lacunarity parameter, as in most

of the previous technical papers dealing with polyadic Cantor fractals in engineering applications [14, 18]. The similarity dimension of all polyadic Cantor fractals is $D = \ln(N)/\ln(\gamma^{-1}) = -\ln(N)/\ln(\gamma)$, which is independent of the lacunarity parameter. The three parameters of a polyadic Cantor set must satisfy certain constraints in order to avoid overlapping between the copies of the initiator. On the one hand, the maximum value of the scaling factor depends on the value of N , such that $0 < \gamma < \gamma_{\max} = 1/N$. On the other hand, for each value of N and γ , there are two extreme values for ε . The first one is $\varepsilon_{\min} = 0$, for which the highest lacunar fractal is obtained, i.e., that with the largest possible gap. For even N , the central gap has a width of $1 - N\gamma$, and for odd N , both large gaps surrounding the central well have a width of $(1 - N\gamma)/2$. The other extreme value is

$$\varepsilon_{\max} = \begin{cases} \frac{1 - N\gamma}{N - 2}, & \text{even } N, \\ \frac{1 - N\gamma}{N - 3}, & \text{odd } N, \end{cases}$$

where for even (odd) N two (three) wells are joined together in the center, without any gap in the central region. The width of the $N - 2$ gaps in this case is equal to ε_{\max} . Thus the corresponding lacunarity is lower than that for $\varepsilon = 0$, but not the smallest one, which is obtained for the most regular distribution, where the gaps and wells have the same width at the first stage ($S = 1$) given by

$$\varepsilon_{\text{reg}} = \frac{1 - N\gamma}{N - 1}.$$

Note that $0 < \varepsilon_{\text{reg}} < \varepsilon_{\max}$.

Polyadic Cantor superlattices have been experimentally grown by Järrendahl et al. [12] by means of properly alternating layers of a-Ge and a-Si. X-ray diffraction techniques were used to analyze the scattering problem of electrons in structures such a $S = 5$ triadic Cantor pre-fractal having 3^6 (729) “elementary” alternating layers. A theoretical analysis of the diffraction peaks has shown good agreement with the results of the experiment. However, a complete analysis requires taking into account both sample imperfections and instrumental limitations, which can influence location, intensity, and profile of the peaks. In this paper, in order to simplify the analysis, these effects are neglected.

3. Estimation of the null positions

The graphical representation of the scattering reflection coefficient as a function of both the particle energy and the lacunarity parameter for polyadic Cantor pre-fractal potentials, referred to as a twist plot, presents a characteristic null structure (black lines and curves) corresponding to energies at which the particle transparently tunnels through the fractal potential wells, i.e., for which the reflection coefficient is null.

The reflection coefficient nulls may be separated in three main families. The first and most noticeable is the family of vertical nulls, being caused by the bound states of

the particle in each potential well, being thus independent of the lacunarity parameter. The nulls in the second family, denoted as arc nulls, are concave upward and curve from the upper left of the twist plots to the lower right. The third family of nulls, referred to as striation nulls, form the finer structure of the twist plots being curves which are concave downward, running from the lower left to the upper right of each twist plot.

The nulls may be calculated from first principles as previously done in Ref. [14] for the interference of light in dielectric fractal superlattices, where only the final mathematical expression is presented, completely omitting the details of the derivation. In the next subsections this gap is filled for quantum fractal superlattices.

3.1. Transfer matrix method

The scattering problem for polyadic Cantor sets with variable lacunarity can be easily solved by means of the transfer matrix method using an effective mass for the electrons. Let us summarize the main details of this widely known technique.

The quantum scattering of particles on one-dimensional potential wells is governed by the steady-state, linear Schrödinger equation

$$-\frac{\hbar^2}{2m^*} \frac{\partial^2 \psi(x)}{\partial x^2} + V(x) \psi(x) = E \psi(x), \quad (1)$$

where $\psi(x)$, m^* and E are the particle wavefunction, effective mass and energy, respectively, \hbar is Planck's constant, and $V(x)$ describes a distribution of potential wells, from here on, taken as a piecewise constant function. The wavefunction ψ_i on the region where the potential constant value is V_i , is the addition of two plane waves, $\psi_i(x) = \psi_i^+(x) + \psi_i^-(x)$, given by

$$\psi_i^\pm(x) = A_i^\pm e^{\pm i k_i x}, \quad k_i = \frac{1}{\hbar} \sqrt{2m^*(E - V_i)},$$

where $i = \sqrt{-1}$, k_i is the local particle momentum, and A_i^\pm are integration constants to be determined by applying the standard boundary conditions at the interfaces between successive wells. In this paper, a distribution of potential wells of the same depth is considered, so the potential $V_i = -V$ in the wells and $V_i = 0$ outside them.

The solution of Eq. (1) for a distribution of N constant potential wells is easily obtained by means of the transfer matrix method [6, 7, 9, 8, 15], yielding

$$\begin{pmatrix} A_0^+ \\ A_0^- \end{pmatrix} = M \begin{pmatrix} A_{N+1}^+ \\ A_{N+1}^- \end{pmatrix}, \quad M = D_0^{-1} \left(\prod_{i=1}^N D_i P_i(d_i) D_i^{-1} \right) D_{N+1}, \quad (2)$$

where

$$D_i = \begin{pmatrix} 1 & 1 \\ k_i & -k_i \end{pmatrix}, \quad P_i(d_i) = \begin{pmatrix} e^{i k_i d_i} & 0 \\ 0 & e^{-i k_i d_i} \end{pmatrix},$$

where d_i is the width of the i -th potential well.

Both the reflection and transmission coefficients of the scattering of a quantum particle, incoming from the left, with the N -well potential is determined by the coefficients of the matrix M ,

$$\begin{pmatrix} A_0^+ \\ A_0^- \end{pmatrix} = \begin{pmatrix} M_{11} & M_{12} \\ M_{21} & M_{22} \end{pmatrix} \begin{pmatrix} A_{N+1}^+ \\ 0 \end{pmatrix},$$

where no backward particle can be found on the right side of the potential, so $A_{N+1}^- = 0$. Both the reflection and transmission coefficients [19] are given by

$$R = \frac{|A_0^-|^2}{|A_0^+|^2} = \frac{|M_{21}|^2}{|M_{11}|^2}, \quad T = \frac{|A_{N+1}^+|^2}{|A_0^+|^2} = \frac{1}{|M_{11}|^2}, \quad (3)$$

respectively, since $k_{N+1} = k_0$.

3.2. Vertical nulls

The vertical nulls shown in the twist plots are the result of bound states of the particle due to its resonance on every potential well of the Cantor superlattice. Since there are N^S potential wells at the S -th stage pre-fractal, the vertical nulls are very noticeable in the twist plot. Using the transfer matrix method is easy to calculate their exact positions, as shown in the appendix of Ref. [13]. This derivation is repeated here for completeness of the presentation.

Let us consider a quantum well at the S -th stage pre-fractal, whose width is $a = L \gamma^S$, where L is the length of the initiator, separated from the next one by a distance $b = L \epsilon^S = a (\epsilon/\gamma)^S$. For future convenience, let us take a symmetrical configuration in which the quantum well is surrounded by two regions of width $b/2$, which corresponds to $V_0 = V_2 = 0$, $V_1 = -V$, $d_1 = a$, and $d_0 = d_2 = b/2$, in the notation introduced in Section 3.1. The particle momentum at the three constant potential regions may be normalized as

$$k_0 = k_2 = \frac{\sqrt{2m^*E}}{\hbar} = \frac{\phi}{a}, \quad k_1 = \frac{\sqrt{2m^*(E+V)}}{\hbar} = \frac{\sqrt{\phi^2 + \phi_V^2}}{a}, \quad (4)$$

where ϕ and ϕ_V are the (non-dimensional) particle energy and depth of the potential well, respectively. The total scattering matrix is given by

$$M = P_0(b/2) D_0^{-1} D_1 P_1(a) D_1^{-1} D_0 P_2(b/2) = \begin{pmatrix} M_{11} & M_{12} \\ M_{21} & M_{22} \end{pmatrix}, \quad (5)$$

which may be easily calculated to obtain

$$M_{11} = M_{22}^* = e^{i b k_0} \left(\cos(a k_1) + i \frac{k_0^2 + k_1^2}{2 k_0 k_1} \sin(a k_1) \right),$$

$$M_{12} = M_{21}^* = -i \frac{k_0^2 - k_1^2}{2 k_0 k_1} \sin(a k_1),$$

where the asterisk indicates complex conjugate.

The vertical nulls correspond to bound states of the particle inside the potential well, being characterized by a null reflection coefficient, for which Eq. (3) yields

$$\sin(a k_1) = \sin(\sqrt{\phi^2 + \phi_V^2}) = 0,$$

having countably infinite solutions given by

$$\sqrt{\phi_i^2 + \phi_V^2} = i \pi, \quad i = 1, 2, \dots \quad (6)$$

Note that the position of the vertical nulls is independent of both the initiator length and the pre-fractal stage thanks to the normalization of the energy (4).

3.3. Arc nulls

The arc nulls are caused by collective bound states of the particle in any of the $2 N^{S-1}$ copies of the series of $\lfloor N/2 \rfloor$ potential wells wholly on either the right or left side of each of the N^{S-1} copies of the initiator at the S -th stage of the pre-fractal superlattice. Since these collective bound states depend on the distance between individual wells, they are a function of the lacunarity parameter.

The Cayley-Hamilton theorem [20] states that every matrix M satisfies the equation given by its characteristic polynomial which for a 2×2 matrix is given by $p_M(\lambda) = \lambda^2 - \text{tr}(M) \lambda + \det(M)$, where $\text{tr}(M)$ and $\det(M)$ are the trace (sum of the diagonal elements) and determinant, respectively, of the matrix. For the scattering matrix of a potential well, Eq. (5), which is an unitary matrix, $\det(M) = |M_{11}|^2 + |M_{12}|^2 = 1$ and $\text{tr}(M) \in \mathbb{R}$. Without loss of generality, $\text{tr}(M) = 2 \cos(\theta)$, where θ is the Bloch phase, being a real number if $|\text{tr}(M)| \leq 2$ and a complex one otherwise, being pure imaginary only if $\text{tr}(M) > 0$. Therefore, the Cayley-Hamilton theorem yields

$$M^2 = 2 \cos(\theta) M - I,$$

where I is the identity matrix. This equation allows the calculation of the n -th power of the matrix M as

$$M^n = \frac{\sin(n \theta)}{\sin(\theta)} M - \frac{\sin((n-1) \theta)}{\sin(\theta)} I, \quad (7)$$

which can be easily proved by the induction principle, in fact, note that

$$M^{n+1} = M M^n = \frac{\sin(n \theta)}{\sin(\theta)} (2 \cos(\theta)) M - \frac{\sin(n \theta)}{\sin(\theta)} - \frac{\sin((n-1) \theta)}{\sin(\theta)} M,$$

and use the formula $2 \cos(\theta) \sin(n \theta) = \sin((n+1) \theta) + \sin((n-1) \theta)$.

The off-diagonal element $(M^n)_{21}$ of Eq. (7) is

$$(M^n)_{21} = \frac{\sin(n \theta)}{\sin(\theta)} M_{21},$$

hence the reflection coefficient is null for

$$\sin(n \theta) = 0, \quad \sin(\theta) \neq 0, \quad (8)$$

whose countably infinite solutions are the set of Bloch phases given by

$$n \theta_{ij} = (n i + j) \pi, \quad i = 0, 1, 2, \dots, \quad j = 1, 2, \dots, n-1, \quad (9)$$

where $n = \lfloor N/2 \rfloor$ in our case. Note that, in the right-hand side of this expression, π appears multiplied by all the natural numbers except the multiples of n , for which $\sin(n\theta)/\sin(\theta) = n$.

The Bloch phase may be calculated from Eq. (5) which yields

$$\begin{aligned} \text{tr}(M) &= 2 \cos(b k_0) \cos(a k_1) - \frac{k_0^2 + k_1^2}{k_0 k_1} \sin(b k_0) \sin(a k_1) \\ &= \frac{(k_0 + k_1)^2}{2 k_0 k_1} \cos(b k_0 + a k_1) - \frac{(k_0 - k_1)^2}{2 k_0 k_1} \cos(b k_0 - a k_1). \end{aligned}$$

Equation (4) yields $a k_0 = \phi$ and

$$a k_1 = \sqrt{\phi^2 + \phi_V^2} = \phi + \frac{1}{2} \left(\frac{\phi_V}{\phi} \right)^2 + O\left(\left(\frac{\phi_V}{\phi} \right)^4 \right),$$

so for $\phi \gg \phi_V$, $k_0 \approx k_1$ and

$$\text{tr}(M) = 2 \cos(\theta) = 2 \cos(a k_1 + b k_0) + O((k_1 - k_0)^2). \quad (10)$$

Therefore, from Eq. (9), the normalized energy ϕ_{ij} for the arc nulls may be calculated as function of the lacunarity as

$$\begin{aligned} \sqrt{\phi_{ij}^2 + \phi_V^2} + \left(\frac{\varepsilon}{\gamma} \right)^S \phi_{ij} &= \left(i + \frac{j}{\lfloor N/2 \rfloor} \right) \pi, \\ i &= 0, 1, 2, \dots, \quad j = 1, 2, \dots, \lfloor N/2 \rfloor - 1. \end{aligned} \quad (11)$$

Note also that

$$\sin(n\theta) = \sin(n \arccos(\text{tr}(M)/2)) = \frac{\sqrt{4 - \text{tr}(M)^2}}{2} U_n(\text{tr}(M)/2),$$

where $U_n(x)$ is the n -th Chebyshev polynomial of the second kind [7]. The null value of this expression at the arc nulls is straightforwardly checked since

$$\text{tr}(M) = 2 \cos(\theta_{ij}) = 2(-1)^j,$$

where Eq. (9) has been used.

3.4. Striation nulls

The striation nulls are caused by the quantum interference between the $\lfloor N/2 \rfloor$ potential wells on the right with those on the left side in each of the N^{S-1} copies of the initiator at the S -th stage of the pre-fractal superlattice. This interaction is exact for even N and only approximate for odd N due to the presence of the potential well at the center of each copy of the initiator. Obviously, they also are a function of the lacunarity parameter.

Let us start with the even N case. Let c be the distance between the rightmost potential well of the $\lfloor N/2 \rfloor$ wells on the left and the leftmost one of those at the right in every copy of the initiator at the S -th stage, yielding $c = L(1 - N\gamma^S - (N-2)\varepsilon^S)$. The scattering matrix for this problem is \tilde{M}^2 where

$$\tilde{M} = P_0(c/2) M^{\lfloor N/2 \rfloor} P_0(c/2).$$

Equations (8) and (9) for $n = 2$ yield

$$2\tilde{\theta}_i = (2i + 1)\pi, \quad i = 0, 1, 2, \dots,$$

where $\text{tr}(\tilde{M}) = 2 \cos(\tilde{\theta})$, which may be easily calculated from

$$\text{tr}(\tilde{M}) = \text{tr}(M^{\lfloor N/2 \rfloor}) \text{tr}(P_0(c)).$$

Introducing the trace operator into Eq. (7) yields

$$\text{tr}(M^n) = \frac{\sin(n\theta)}{\sin(\theta)} \text{tr}(M) - 2 \frac{\sin((n-1)\theta)}{\sin(\theta)} = 2 \cos(n\theta),$$

hence, using Eq. (10), for $\phi \gg \phi_V$,

$$\text{tr}(\tilde{M}) = 2 \cos(n(a k_1 + b k_0)) 2 \cos(c k_0) + O((k_1 - k_0)^2),$$

yielding $\tilde{\theta} \approx n a k_1 + (n b + c) k_0$, where $n = \lfloor N/2 \rfloor$, resulting in

$$\begin{aligned} \lfloor N/2 \rfloor \sqrt{\phi_i^2 + \phi_V^2} + \left(\gamma^{-S} - N - (N - \lfloor N/2 \rfloor - 1) \left(\frac{\varepsilon}{\gamma} \right)^S \right) \phi_i \\ = (2i + 1) \frac{\pi}{2}, \quad i = 0, 1, 2, \dots, \end{aligned} \quad (12)$$

for the striation nulls for even N .

For the odd N case, the central potential well between both series of $\lfloor N/2 \rfloor$ wells makes their mutual interference not exact. However, an approximate formula may be obtained as easily as before. Let $c = L(1 - N\gamma^S - N\varepsilon^S)$ such that $c/2 + b$ be the distance between the central potential well and that in the right (or left) in every copy of the initiator at the S -th stage. The corresponding scattering matrix is \hat{M}^2 where

$$\hat{M} = P_1(a/2) D_1^{-1} D_0 P_0(c/2) M^{\lfloor N/2 \rfloor} P_0(c/2) D_0^{-1} D_1 P_1(a/2),$$

where the central potential well has been divided in two parts, one located completely to the left and the other one completely to the right. By exactly the same arguments as before, omitted here for brevity, $\text{tr}(\hat{M}) = 2 \cos(\hat{\theta})$, where

$$\hat{\theta} \approx (N - \lfloor N/2 \rfloor) (a k_1 + b k_0) + c k_0,$$

resulting in

$$\begin{aligned} (N - \lfloor N/2 \rfloor) \sqrt{\phi_i^2 + \phi_V^2} + \left(\gamma^{-S} - N - (\lfloor N/2 \rfloor - 1) \left(\frac{\varepsilon}{\gamma} \right)^S \right) \phi_i \\ = (2i + 1) \frac{\pi}{2}, \quad i = 0, 1, 2, \dots, \end{aligned} \quad (13)$$

as an approximation for the striation nulls for odd N .

Note that Eq. (12) is a particular case of Eq. (13), hence in Ref. [14] only the last one is shown for both even and odd N .

4. Presentation of results

Twist plots are the gray-scale representation of the scattering reflection coefficient (in decibels, i.e., $10 \log_{10} R$) as a function of the normalized energy (ϕ) and the lacunarity parameter (ε). Here, a linear gray scale was used, from black for null values to white for the maximum value equal to unity. Figures 2 (a) and 3 (a) show twist plots for, respectively, pentadic ($N = 5$) and hexadic ($N = 6$) Cantor fractal potential both with $S = 1$, $\gamma = 1/7$, and $\phi_V = 1/2$. The horizontal interval covers the normalized energy ϕ from 0 to $\sqrt{(3\pi)^2 - \phi_V^2} \approx 9.41$, the energy of the third vertical null line. These figures have been obtained by a straightforward numerical implementation of the transfer matrix method.

The most noticeable fact in Figs. 2 (a) and 3 (a) is the null structure (black lines and curves) corresponding to energies at which the particle transparently tunnels through the fractal potential wells. The strongest (darkest) among these curves are the vertical nulls. The arc nulls, which are concave upward, curving from the upper left to the lower right of the plots, appear in pairs for $N = 6$ (see Fig. 3 (a)), as expected from Eq. (11). The striation nulls, which are concave downward, running from the lower left to the upper right of each twist plot, form the finer structure of the twist plots.

The main difference between Figs. 2 (a) and 3 (a) is observed for $N = 5$ and, in general, for odd N , because in such a case the tunnelling is not perfectly transparent at the whole length of the arc nulls, but instead appear dashed, alternatively darker and lighter after they cross the striation nulls. The striation nulls also appear lighter when they cross the arc nulls, resulting in a leopard-like spot pigmentation pattern. This result is not unexpected, since both the arc and the striation nulls are not truly

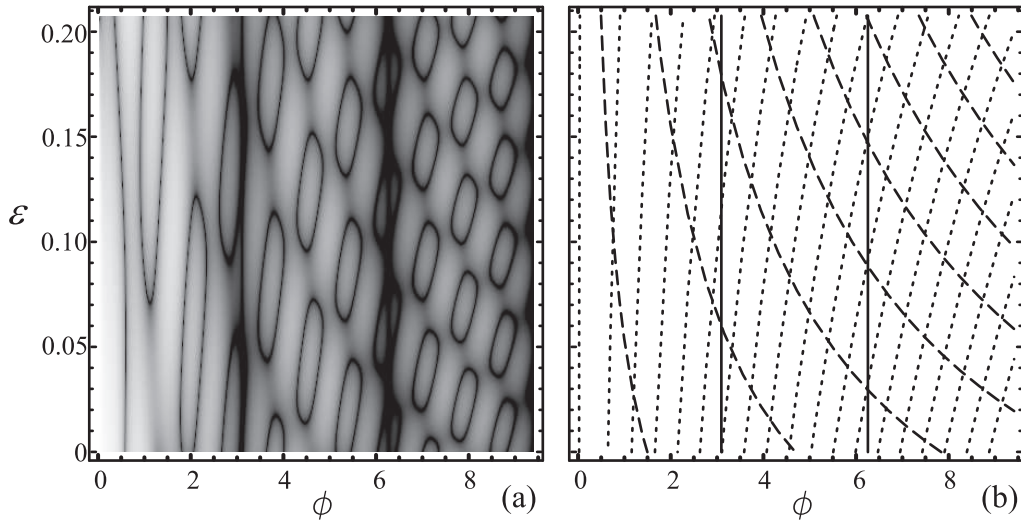


Figure 2. Scattering reflection coefficient (a) for the polyadic Cantor pre-fractal potentials with $S = 1$, $N = 5$, $\gamma = 1/7$, and $\phi_V = 1/2$, and the analytical curves (b) for the corresponding vertical (continuous line), arc (dashed line), and striation (dotted line) nulls.

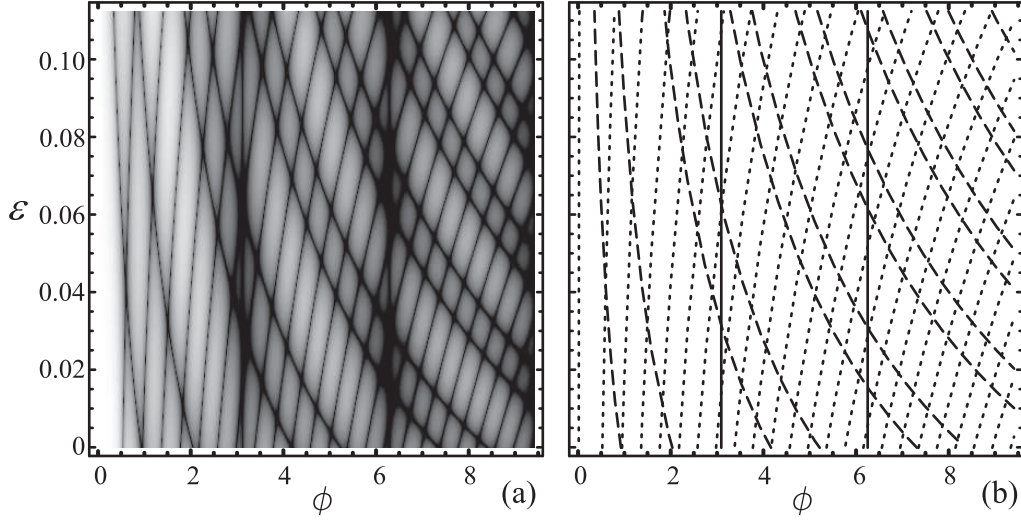


Figure 3. Scattering reflection coefficient (a) for the polyadic Cantor pre-fractal potentials with $S = 1$, $N = 6$, $\gamma = 1/7$, and $\phi_V = 1/2$, and the analytical curves (b) for the corresponding vertical (continuous line), arc (dashed line), and striation (dotted line) nulls.

null for odd N due to the single quantum well between each pair of $\lfloor N/2 \rfloor$ potential wells, which introduces non-periodicity in the scattering problem resulting in a (small) non-null reflection coefficient.

The nulls calculated by Eqs. (6), (11), and (13), are shown in Figs. 2 (b) and 3 (b). These figures clearly show the good accuracy of the analytical approximations which reproduce the main features of the corresponding twist plots. For even N the accuracy is surprisingly good. For odd N , as expected, both arc and striation nulls are less accurate. Note also that the accuracy degrades for small energy as expected due to the lack of validity of the approximations used in Sections 3.3 and 3.4 in such a case.

5. Conclusions

Analytical expressions for the calculation of the particle energy for transparent tunnelling in polyadic Cantor pre-fractal potentials as a function of the lacunarity parameter have been obtained from first principles by using the transfer matrix method. The comparison with the results obtained by a numerical implementation of the transfer matrix method shows the good accuracy of these expressions for N -adic Cantor pre-fractals with even N and their reasonable accuracy for odd N . The reasons for this difference in accuracy have also been presented in detail.

The analytical results obtained in this paper can be easily incorporated as a complement in computer laboratories for undergraduate quantum mechanics or solid-state physics courses currently using the transfer matrix method only as a numerical tool [15, 13]. In fact, the possibility of approximately calculating the geometrically complex figures observed in the results provides the student with an excellent example

of the combination of theory and numerical experiments. Thus, different aspects of the model may be assigned to different students or groups of students. In fact, stimulating discussions among the students follow naturally from this kind of approach.

Finally, since the transfer matrix methods may be adapted by physics analogy to the propagation of waves in general one-dimensional quasiperiodic media [21], the present results may be also applied to, for example, acoustics, optics, or vibrating strings. In fact, the effect of the lacunarity in the scattering on generalized Cantor media was first studied in optics [14, 18], where the additional degree of freedom introduced by the lacunarity was used with success to obtain new physical characteristics. A detailed study of these applications, outside the scope of this paper, may also be an stimulating topic for further study.

Acknowledgments

This work has been supported by the Ministerio de Educación y Ciencia (grant FIS2005-01189), Spain. We also acknowledge the financial support from the Universidad Politécnica de Valencia (Vicerrectorado de Innovación y Desarrollo, Programa de Incentivo a la Investigación 2005), Spain.

References

- [1] Nag B R 2002 *Physics of quantum well devices* (Berlin: Springer-Verlag)
- [2] Roblin P 2002 *High-speed heterostructure devices: From device concepts to circuit modeling* (Cambridge, UK: Cambridge University Press)
- [3] Kolbas R M and Holonyak N Jr 1984 *Am. J. Phys.* **52** 431
- [4] Mazurczyk R 1999 *Chaos Solitons Fract.* **10** 1971
- [5] Nawrocki M and Gaj J A 1984 *Am. J. Phys.* **52** 807
- [6] Kalotas T M and Lee A R 1991 *Eur. J. Phys.* **12** 275
- [7] Sprung D W L, Wu H, and Martorrell J 1993 *Am. J. Phys.* **61** 1118
- [8] Sprung D W L, Sigetich J D, Wu H, and Martorrell J 2000 *Am. J. Phys.* **68** 715
- [9] Walker J S and Gathright J 1994 *Am. J. Phys.* **62** 408
- [10] Herman M A and Sitter H 1989 *Molecular beam epitaxy: Fundamentals and current status* (Berlin: Springer-Verlag)
- [11] Axel F and Terauchi H 1991 *Phys. Rev. Lett.* **66** 2223
- [12] Järrendahl K, Dulea M, Birch J, and Sundgren J-E 1995 *Phys. Rev. B* **51** 7621
- [13] Monsoriu J A, Villatoro F R, Marín M J, Pérez J, and Monreal L 2006 *Am. J. Phys.* **74** 831
- [14] Jaggard A D and Jaggard D L 1998 *J. Opt. Soc. Am. A* **15** 1626
- [15] Monsoriu J A, Villatoro F R, Marín M J, Urchueguía J F, and Fernández de Córdoba P 2005 *Eur. J. Phys.* **26** 603
- [16] Hurt A J 1988 *Am. J. Phys.* **56** 969
- [17] 1983 Mandelbrot B B *The Fractal Geometry of Nature* (New York: Freeman)
- [18] Monsoriu J A, Saavedra G, and Furlan W D 2004 *Opt. Express* **12** 4227
- [19] Liboff R 2003 *Introductory Quantum Mechanics* (Redwood City, CA: Benjamin Cummings)
- [20] Meyer C 2001 *Matrix Analysis and Applied Linear Algebra* (Philadelphia, PA: SIAM)
- [21] Griffiths D J and Steinke C A 2001 *Am. J. Phys.* **69** 137